**Supplementary Information**

**Abbreviations**

| | |
|---|---|
| Ads_dos: | Adsorbent dosage |
| ANN: | artificial neural networks |
| BET: | Brunauer–Emmett–Teller |
| CGW: | Carbonized garment waste biochars |
| CGW400: | CGW was carbonized at temperatures of 400 $^{o}$C |
| CGW600: | CGW was carbonized at temperatures of 600 $^{o}$C |
| CGW800: | CGW was carbonized at temperatures of 800 $^{o}$C |
| CGW900: | CGW was carbonized at temperatures of 900 $^{o}$C |
| Cr: | Chromium |
| Cr_con: | Cr ion concentration |
| EDX: | Energy-Dispersive X-ray Spectroscopy |
| FTIR: | Fourier Transform Infrared Spectroscopy |
| LR: | Linear Regression |
| MAE: | Mean Absolute Error |
| ML: | Machine learning |
| RF: | Random forests |
| RMSE: | Root Mean Square Error |
| $R^2$: | Coefficient of determination |
| SEM: | Scanning Electron Microscopy |
| SVM: | Support vector machines |
| Pb: | Lead |
| Pb_con: | Pb ion concentration |
| PFO: | Pseudo-first-order |
| PSO: | Pseudo-second-order |
| $q_e$: | Adsorption capacity |
| $q_{m,cal}$: | Calculated adsorption capacity |
| $q_{e,exp}$: | Experimental adsorption capacity |
| XRD: | X-ray Diffraction |
| Time: | Contact time |

**SI-1: Pyrolysis reactor description**

The reactor consists of a cylindrical stainless-steel chamber (Inox 304) with a total height of 1.68 m and an internal diameter of 0.77 m, providing a total working capacity of 12 kg of

garment waste per batch. The inner wall is insulated with a 10–15 cm refractory ceramic layer to minimize heat loss and maintain stable thermal conditions during operation. The lower section of the reactor houses the primary combustion chamber, which is fueled by liquefied petroleum gas and is connected to an adjustable air supply valve that precisely regulates combustion intensity and airflow.

A distinctive feature of this design is the incorporation of an organic vapor recirculation loop that continuously redirects volatile gases and organic vapors generated during pyrolysis back into the combustion zone. This feedback mechanism provides 30–50% of the total heating energy, thereby reducing external fuel consumption and improving overall energy efficiency. An exhaust gas outlet is installed to safely discharge non-condensable gases. At the same time, thermocouples (type K, ± 1 °C accuracy) are embedded at multiple points within the chamber to monitor and control temperature profiles in real time.

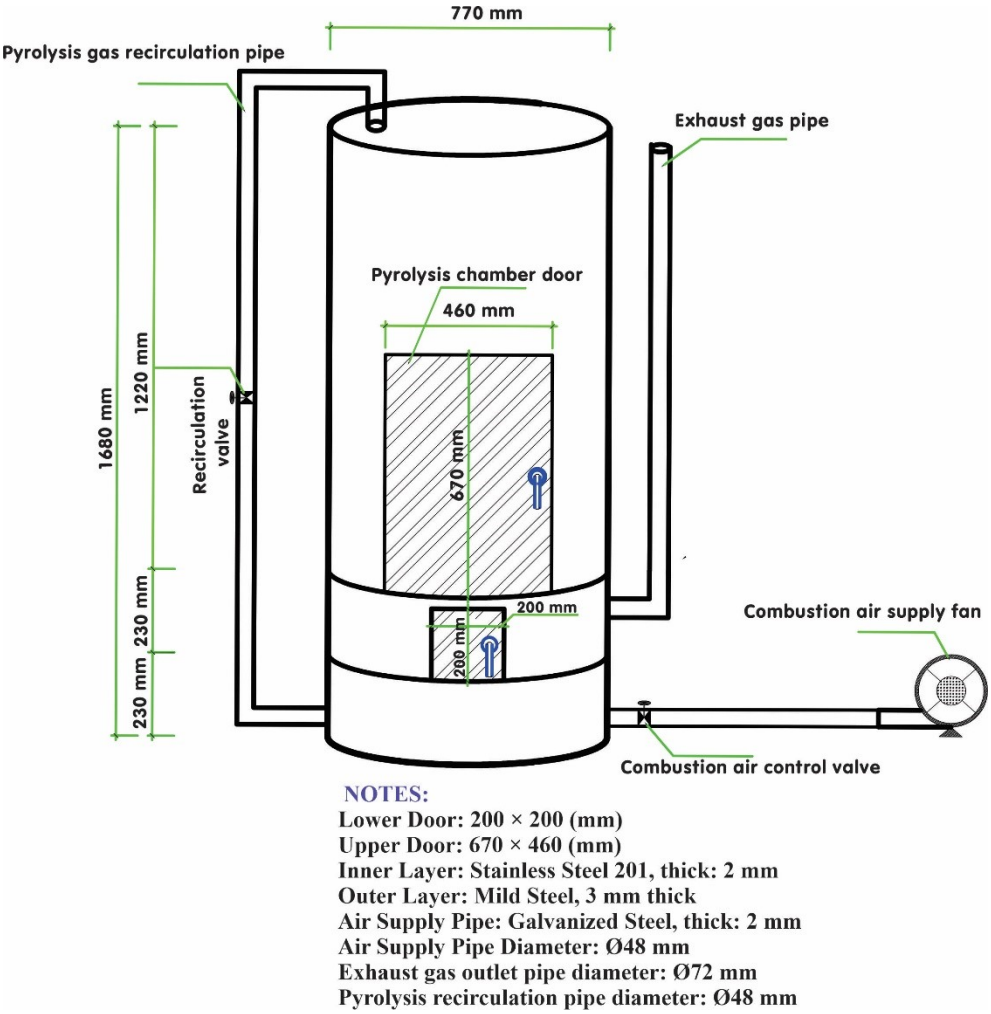


**Fig. S1.** Schematic design of the vertical anaerobic pyrolysis reactor for converting garment waste into multifunctional materials

**SI-2: Adsorption equations**

The adsorption capacity of CGW at a specific contact time ($q_t$, mg/g) and at equilibrium ($q_e$, mg/g) was determined using equations (1) and (2):

$$q_e = \frac{(C_o - C_e)V}{W} \quad (1)$$

$$q_t = \frac{(C_o - C_t)V}{W} \quad (2)$$

where $C_o$, $C_t$, and $C_e$ (mg/L) denote the initial, time-dependent and equilibrium concentrations of Pb(II) or Cr(VI) in solution, respectively; $V$ (L) is the volume of the metal solution, and $W$ (g) is the dry weight of the biochar adsorbent.

To investigate the adsorption rate and mechanism, the kinetic data were fitted using three established models: the pseudo-first-order, pseudo-second-order and Elovich models. Their respective linearized equations are expressed using equations (3), (4) and (5):

$$\text{Pseudo - first - order model: } \ln(q_e - q_t) = \ln q_e - k_1 t \quad (3)$$

$$Pseudo - second - order\ model: \frac{t}{q_t} = \frac{1}{k_2 q_e^2} + \frac{1}{q_e} t \quad (4)$$

$$Elovich\ model: \frac{t}{q_t} = \frac{1}{\beta} ln(\alpha\beta) + \frac{1}{\beta} lnt \quad (5)$$

In these equations, $q_e$ and $q_t$ (mg/g) represent the adsorption capacities at equilibrium and at time $t$ (min), respectively. $k_1$ ($min^{-1}$) and $k_2$ ($g \cdot mg^{-1} \cdot min^{-1}$) are the rate constants for the pseudo-first-order and pseudo-second-order models. In the Elovich equation, $\alpha$ ($mg \cdot g^{-1} \cdot min^{-1}$) corresponds to the initial adsorption rate, while $\beta$ ($g \cdot mg^{-1}$) reflects the degree of surface coverage and activation energy associated with chemisorption.

By comparing the regression coefficients ($R^2$) and the agreement between experimental and theoretical $q_e$ values, the dominant adsorption mechanism - whether physisorption or chemisorption - was determined.

Equilibrium adsorption data for Pb(II) and Cr(VI) were further analyzed using three classical isotherm models - Langmuir, Freundlich, and Sips - to describe the interactions between the metal ions and the heterogeneous surface of CGW. The corresponding model equations are given as equations (6), (7), and (8):

$$Langmuir\ model: q_e = \frac{q_m K_L C_e}{1 + K_L C_e} \quad (6)$$

$$Freundlich\ model: q_e = K_F C_e^{\frac{1}{n}} \quad (7)$$

$$Ship\ model: q_e = \frac{q_m (bC_e)^{\frac{1}{n}}}{1 + (bC_e)^{\frac{1}{n}}} \quad (8)$$

Where, $q_e$ (mg/g) and $q_m$ (mg/g) are the equilibrium and maximum adsorption capacity of the adsorbents, respectively; $b$ is the Langmuir constant related to the free adsorption energy (L/mg); $C_e$ is the equilibrium concentration of Pb(II) or Cr(VI) (mg/L); $K_L$ (L/mg) is the Langmuir constant; $K_F$ (mg/g) is the Freundlich constant; $n$ is the adsorption intensity.

Here, $q_e$ (mg/g) and $q_m$ (mg/g) represent the equilibrium and maximum adsorption capacities, respectively. $C_e$ (mg/L) denotes the equilibrium concentration of Pb(II) or Cr(VI). $K_L$ (L/mg) is the Langmuir affinity constant related to the free energy of adsorption, $K_F$ ($(mg \cdot g^{-1})(L \cdot mg^{-1})^{1/n}$). N are the Freundlich constants associated with adsorption capacity and intensity. In contrast, $b$ and $n$ in the Sips model correspond to the heterogeneity and energy distribution of the surface binding sites.

**SI-3: Machine learning**

The dataset was partitioned into training (80%) and testing (20%) subsets using stratified random sampling via the caret::createDataPartition() function (seed = 42) [1] to ensure proportional representation of adsorption capacity values. Data preprocessing included centering and scaling for Linear Regression (LR) and Random Forest (RF) models, and min–max normalization to [0,1] for Support Vector Machine (SVM) models using caret::preprocess(). This structured preprocessing ensured numerical stability, improved model convergence and enhanced comparability across algorithms.

Four supervised learning algorithms were applied to predict the adsorption capacity of Pb(II) and Cr(VI): ANN, LR, RF and SVM. Each model was trained, tuned and validated using 10-fold cross-validation to prevent overfitting.

Artificial Neural Network (ANN): A single-hidden-layer neural network was trained using the caret::nnet package. Grid search optimization was performed over hidden layer sizes (2–20 nodes), with a fixed decay = 0.01 and maxit = 50,000 iterations. The optimal model consisted of four hidden neurons, achieving high convergence stability and predictive accuracy. Linear Regression (LR): Implemented via ordinary least squares, the LR model served as a baseline due to its interpretability and minimal computational cost. No hyperparameter tuning was required. Random Forest (RF): The RF model was constructed using the caret::rf package, with a 10-fold cross-validation grid search over mtry (1–4) and min.node.size (1, 2, 4), maxdepth (10, 20, 30, unlimited), and ntree (100, 500, 1000). The optimal configuration was mtry = 2, ntree = 500, nodesize = 5, and maxnodes = NULL,

providing a strong balance between bias and variance. Support Vector Machine (SVM): The SVM model, implemented via the e1071 package, underwent random search optimization across kernel types (linear, polynomial, radial), cost parameter C (0.01–10), gamma (0.001–0.1), and polynomial degree (1–3). The best performance was achieved with a polynomial kernel, C = 10, degree = 3, gamma = 0.1, and epsilon = 0.1. Each model was evaluated with a fixed random seed (42) to ensure reproducibility. The final trained models were benchmarked against each other based on their predictive performance metrics.

The performance of all models was quantitatively assessed using three standard statistical metrics: Coefficient of determination ($R^2$), Root Mean Square Error (RMSE), and Mean Absolute Error (MAE). These were computed according to Equations (9)–(11):.

$$R^2 = 1 - \frac{\sum_{i=1}^{n}(y_i - \hat{y}_i)^2}{\sum_{i=1}^{n}(y_i - \bar{y})^2} \quad (9)$$

$$RMSE = \sqrt{\frac{1}{n}\sum_{i=1}^{n}(y_i - \hat{y}_i)^2} \quad (10)$$

$$MAE = \frac{1}{n}\sum_{i=1}^{n}\left|y_i - \hat{y}_i\right| \quad (11)$$

where $y_i$ denotes the experimentally measured adsorption capacity, $\hat{y}_i$ is the predicted value, $\bar{y}$ represents the mean of observed values, and $n$ is the total number of samples.

The $R^2$ value indicates the proportion of variance in the experimental data explained by the model; values approaching 1.0 indicate a superior model fit. The RMSE provides a quadratic measure of prediction deviation, emphasizing larger errors, while the MAE quantifies the mean absolute deviation, offering a linear measure of overall prediction accuracy [2]. By integrating these complementary metrics, a comprehensive evaluation of each model's robustness, generalization, and predictive precision was achieved.

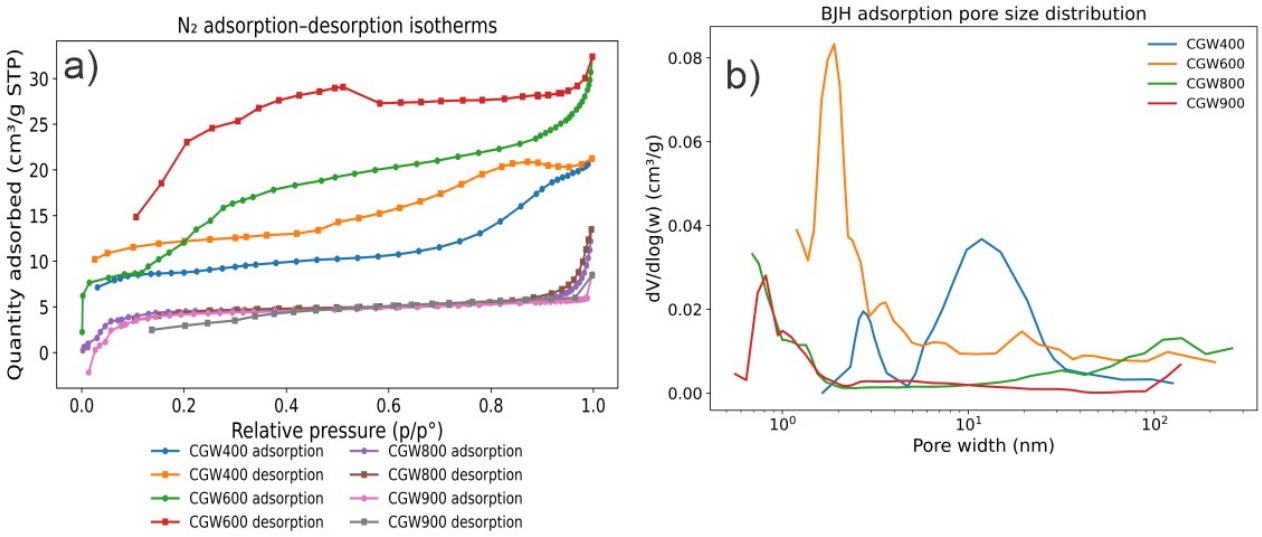


**Fig. S2.** (a) Nitrogen adsorption–desorption isotherms and (b) pore size distribution curves of CGW400, CGW600, CGW800 and CGW900

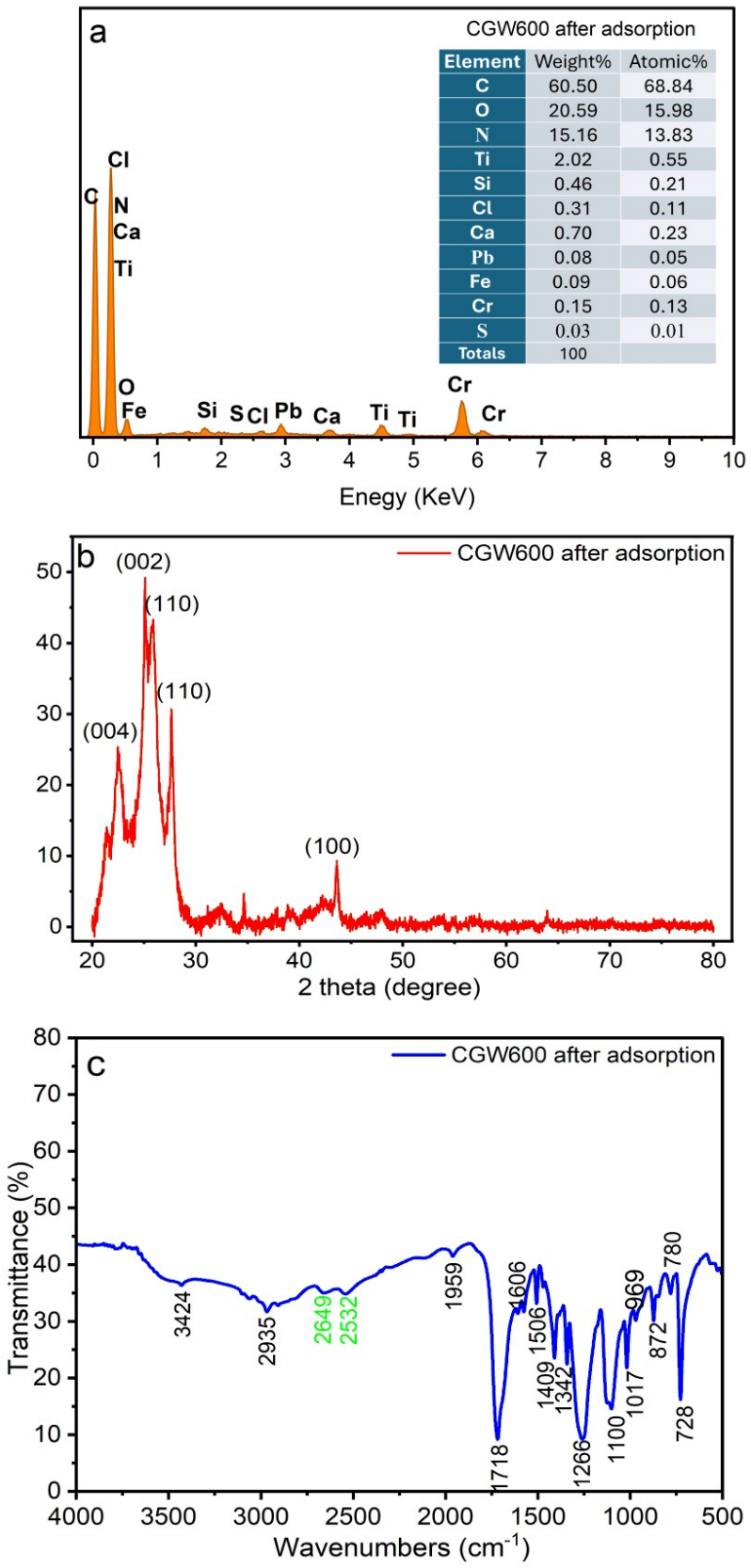


**Fig. S3.** EDX spectra (a), XRD (b) and FTIR (c) of CWG600 afrer Pb and Cr adsorption

References

1 R. T. Schossler, S. Ojo, Z. Jiang, J. Hu and X. Yu, *Sci. Rep.*, 2024, **14**, 1–15.

2 E. Vakarelska, M. Nedyalkova, M. Vasighi and V. Simeonov, *Chemosphere*, 2022, **287**, 132189.